RSC
Sustainability

ROYAL SOCIETY
OF **CHEMISTRY**

PAPER
V. Bressi *et al.*
Hydrochar from *Sargassum muticum*: a sustainable
approach for high-capacity removal of Rhodamine B dye

Check for updates

Hydrochar from *Sargassum muticum*: a sustainable approach for high-capacity removal of Rhodamine B dye†

D. Spagnuolo, [ID] [a] D. Iannazzo, [b] T. Len, [c] A. M. Balu, [ID] [c] M. Morabito, [a] G. Genovese, [ID] [a] C. Espro [b] and V. Bressi [ID] *[bc]

In this study, an environmentally friendly protocol for the recovery of hydrochar by hydrothermal carbonization (HTC) of the macroalga *Sargassum muticum* was presented. HTC conditions such as temperature (180–300 °C) and reaction time (60–300 min) were investigated to study the differences between the obtained samples and find the optimal conditions that maximize the yield of hydrochar. The acquired results demonstrate that the highest hydrochar yield is reached after 180 min at a reaction temperature of 180 °C. The obtained biocarbons were characterized by several techniques (XRD, FTIR, XPS, SEM-EDX, and BET) and their adsorption capability was evaluated in the environmental recovery of water organic pollutants.

Sustainability spotlight

This work is aligned with the United Nations' 17 sustainable development goals, specifically SDG6, which emphasizes the importance to ensure access to sustainable and clean water, and SDG12, which aims to reduce waste impact through upgrading processes. The aim of this research is to enhance the invasive algae-biomass that can pose a threat to human health and marine ecosystems, by converting it into valuable carbonaceous materials by developing a simple, and eco-friendly hydrothermal process. Furthermore, in line with SDG13 that aims to reduce the impact of climate change and SDG14, which promotes the well-being of aquatic life and its inhabitants, the resulting hydrochar has been exploited as an adsorbent to remove the harmful pollutant Rhodamine B, without requiring any activation that may involve severe treatment conditions, demonstrating that it could enable the rapid and selective detection and adsorption of pollutants in water.

1 Introduction

Algae represent an artificial cluster of aquatic plants without a formal taxonomy standing, including polyphyletic photosynthetic organisms ranging from unicellular to complex multicellular thalli.[1] Macroalgae (*i.e.*, multicellular forms) are interesting natural sources of chemical compounds with antioxidant, anti-inflammatory, antimicrobial, and anticancer activity,[2–5] but macroalgae living in transitional ecosystems, such as man-made coastal environments, produce large amounts of waste that must be removed regularly.[2,6] The Lagoon of Venice is a shallow coastal water body affected by an array of anthropogenic factors[7] that may facilitate the settlement and growth of allochthonous (alien) species, able to overwhelm native vegetation. The brown macroalga *Sargassum muticum* (Phaeophyceae) is considered an alien species in Venice Lagoon, growing mainly on the docks of the historical centre. *Sargassum muticum* reaches densities such as to appear as continuous belts difficult to dispose. The uncontrolled growth of algae can often lead to harmful consequences for the environment and the need to dispose of them becomes a significant problem.[8] The collection of the invasive species and their conversion into bioactive compounds with high added value represents a possible strategy to mitigate their negative impacts on the environment.[6]

Biomasses represent an excellent ally of green chemistry thanks to the renewable and biocompatible raw materials, rather than exhaustible, resulting in the reduction of waste. In recent years, natural wastes have become promising renewable raw materials for the production of chemicals, fuels, and energy that are not exhaustible, which has led to the reduction of wastes becoming the main topic of numerous research studies.[9] One of the main drawbacks of using biomass is its high moisture content.[10] However, especially with lignocellulosic materials, it is necessary to modify the feedstock by physical or

[a]Department of Chemical, Biological, Pharmaceutical and Environmental Sciences, University of Messina, Viale F. Stagno d'Alcontres 31, 98166 Messina, Italy

[b]Department of Engineering, University of Messina, Contrada di Dio–Vill. S. Agata, I-98166 Messina, Italy. E-mail: viviana.bressi@unime.it

[c]Department of Organic Chemistry, University of Córdoba, Campus de Rabanales, Marie Curie (C-3), Ctra Nnal IV-A, Km 396, Cordoba, Spain

chemical pre-treatments in order to meet the requirements of thermochemical conversion processes.

In this context, hydrothermal carbonization (HTC) is one of the favourable thermochemical approaches for treating biomass with high moisture content.[11] The process consists of a thermic degradation of the natural feedstock in water media under mild conditions sufficient to cause dehydration and decarboxylation processes[12] and to convert biomass into a solid carbon-rich material.[13] At the end of the treatment, generally 50–80% of the starting material is converted into a solid product, 5–20% into a liquid product with a high content of soluble organic and inorganic compounds and the remaining percentage into gas which is mainly composed of CO_2.[14] The variability of the percentages of the resulting products depends on the starting material and on the process conditions. The produced solid is identified by several names, including green coal, biochar, hydrochar, and charcoal.[15] Recent studies demonstrated that HTC is a promising technology for upgrading biomass into liquid biofuels,[16] soil amenders,[17] carbon materials for liquid contaminant adsorption,[18] nanocarbon materials,[19,20] catalysts or photocatalysts,[21] or into carbon materials for increasing the fuel cell efficiency.[19]

The current methods employed for treating water contaminated with organic pollutants include a range of several approaches such as chemical processes, (*i.e.* oxidation and photodegradation), biological processes, including microbial biomass adsorption and decolourization, and physical processes like membrane filtration and adsorption. However, chemical processes are hindered by their high operating costs, extensive energy consumption, and the potential generation of undesired by-products.[22] Biological processes necessitate extended residence times and cannot ensure stability due to the nature of microorganisms.[23] Interestingly, physical processes like adsorption offer a cost-effective solution with excellent removal efficiency demonstrated for several pollutants.[24] Indeed, adsorption using highly porous activated carbons is one of the many methods used to detect dye-polluted wastewater harmful to human health because of its simplicity, speed and high efficiency.[25] In addition, with the development of industry, dyes are directly or indirectly discharged into water,[26] which has dangerous and harmful consequences to the environment and is fatal to humans if ingested. Among the harmful substances, Rhodamine B has been classified as a possible human carcinogen by the International Agency for Research on Cancer (IARC).[27] Prolonged exposure to Rhodamine B has been linked to an increased risk of cancer development. Recent studies have shown that exposure to Rhodamine B can lead to organ dysfunction and impairment.[28,29] Furthermore, Rhodamine B can affect fertility, cause reproductive abnormalities, and hinder proper fetal development. Importantly, rhodamine B is known to be harmful to aquatic life, thus causing an environmental impact. Its release into water bodies can result in pollution and harm aquatic organisms, disrupting ecosystems.[30]

One of the most common uses of hydrochar is its high adsorption capacity for various pollutants in water.[31] However, hydrochars are usually subjected to chemical or physical activation processes to increase their adsorption capability.[32] In a recent study, Hou *et al.*[33] successfully synthesized highly porous hydrochars through hydrothermal carbonization of bamboo shoot shells, and achieved a remarkable Rhodamine B adsorption capacity of 85.8 mg g^{-1} at 25 °C, highlighting the significant adsorption potential of non-activated hydrochar. In a more recent study,[34] different lignocellulosic biomasses underwent HTC, and the adsorption potential was assessed by modulating the N-doping using various green sources. The resulting hydrochars exhibited impressive adsorption capacities for methylene blue and congo red, measuring 57.52 mg g^{-1} and 62.19 mg g^{-1}, respectively, demonstrating the feasibility of obtaining hydrochars with high adsorption capacities through hydrothermal processes. Moreover, the study highlights the significance of nitrogen groups in the adsorption process, as they contribute to increased binding between the adsorbate and adsorbent.

In this study, different HTC conditions of temperature and reaction time and the solid products were extensively studied in order to understand how the variables affected the final properties of the hydrochars obtained from the hydrothermal treatment of the macroalga *Sargassum muticum*. The resulting hydrochars show promising properties such as macroporous area, high carbon content, and interesting functional groups, resulting in high efficient adsorption without any chemical-physical activation for the removal of the Rhodamine B water dye-pollutant.

2 Experimental

2.1 Materials and sample collection

Thalli of *Sargassum muticum* were collected in Venice Lagoon, Italy (45° 25′ 42.6″ N – 12° 19′ 50.7″ E) (Fig. S1† shows the picture of the collected raw material). The algae was immediately rinsed with seawater to remove any possible debris, sand and organisms. The cleaned biomass was placed in plastic containers at low temperature and transported to the laboratory. A second washing step was performed with tap water to remove surface salt. Then, the algae was dried at 40 °C in an oven before storage at – 20 °C to decrease the degradation rate. The chemical composition of algae *Sargassum muticum* has been extensively studied and is reported in Table S1.†

A portion of the sample was desiccated as a voucher herbarium specimen, the epiphytes were removed manually, and the sample was dried in silica gel and kept at – 20 °C for molecular identification (DNA barcoding).

2.2 Hydrothermal carbonization (HTC) process

A mixture of defrosted thalli of *Sargassum muticum* (5 g of dry starting material) and deionized water (100 mL) was placed into a 300 mL stainless steel autoclave (series 4540 Parr Instrument Company, IL, USA). The reactor was heated with a rate speed of 10 °C min^{-1} and the operative reaction times were recorded once the set temperature reached. The process was carried out under stirring, autogenous pressure and a N_2 atmosphere. At the end of the HTC, the reactor was cooled and the solid phase was separated from the liquid by a vacuum filtration setup. The recovered solid was washed several times with distilled water and let to dry for 24 h under vacuum at 100 °C. The obtained hydrochar samples

are here named as SM-HC T–t, with T, the reaction temperatures (180, 240, and 300 °C), and t, the reaction time (60, 180, and 300 min). Subsequently they will be named from SM1 to SM9, to enhance simplicity, with detailed reference to: SM1, SM2, and SM3 the hydrochars obtained after 60 minutes under 180 °C, 240 °C and 300 °C respectively; SM4, SM5, and SM6 the hydrochars obtained after 180 minutes under 180 °C, 240 °C and 300 °C respectively; SM7, SM8, and SM9 the hydrochars obtained after 300 minutes under 180 °C, 240 °C and 300 °C respectively. The yield of the hydrochar was determined using the following formula:

$$\text{mass yield(wt\%)} = \frac{\text{gr of product}}{\text{gr of initial dry SM}} \times 100 \quad (1)$$

The combined effect of time and temperature on the process can be evaluated by the so-called severity factor ($\log R_0$) firstly described by Overend *et al.*[35] In this field, numerous studies have been using this metric since it is also related to the distributions, chemical compositions and properties of the starting materials.[36] Therefore, the role of reaction time and temperatures in the HTC of the algae was deduced by the severity factor which is expressed as:

$$\log_{10} R_0 = \log\left[t \times \exp\left(\frac{T - T0}{14.75}\right)\right] \quad (2)$$

where t is the time (min), T is the temperature (°C), and $T0$ is the reference temperature (generally set at 100 °C).

2.3 Chemical-physical characterization of hydrochar

The study of the functional groups of the obtained materials was carried out by means of Fourier transform infrared (FTIR) spectroscopy using a PerkinElmer Spectrum 100 spectrometer, equipped with a classic ATR sampling unit. The spectra were registered in the range from 4000 to 500 cm^{-1} by performing the analysis at room temperature with accumulation of 30, scanning speed of 2 mm s^{-1}, and resolution of 4.0 cm^{-1}, without any earlier handling. A Bruker D8 Advance A 25 X-ray diffractometer operating at 40 kV and in the range 5–80° 2θ, with an increasing rate of 0.01° s^{-1} was used to study the crystallinity of the obtained hydrochars. The samples' morphology was investigated by scanning electron microscopy (SEM) using a Zeiss 1540XB FE SEM-EDX (Zeiss, Germany) apparatus operating at 10 kV. Prior to analysis, the algae and the hydrochars were dried and kept at 85 °C in a vacuum oven overnight. The textural properties of the synthesized materials were determined by the Brunauer–Emmett–Teller (BET.) method from N$_2$ isotherms recorded at 77 K by using a Quantachrome® ASiQwin™ apparatus (Anton Paar Companies, Graz, Austria). X-ray photoelectron spectroscopy (XPS) was developed by using an XPS SPECS PHOIBOS150 MCD surface analysis system with an X-ray source with Mg and Al anodes, and Al and Ag monochromatic sources.

2.4 Adsorption tests

The adsorption efficiency of the hydrochars SM1, SM2, and SM3 for Rhodamine B removal was assessed *via* dispersing different

amounts of hydrochars into 50 mL of Rhodamine B solutions 50 μM under stirring (350 rpm) by monitoring the adsorbent amount (5, 10, 30, 50, and 100 mg), the contact time (5, 15, 30, and 60 minutes) and the temperature (25, 35, and 45 °C). The samples were filtered and their absorbance was measured by using a UV-Vis spectrophotometer (PerkinElmer, Lambda 365). All the measurements were repeated three times and all the adsorption spectra were fitted by corresponding linear models. The calculation of pollutant removal percentage was determined using the following empirical formula:

$$\text{removal\%} = \frac{(C_0 - C_e)}{C_0} \times 100 \quad (3)$$

where C_0 (mg L^{-1}) represents the initial concentration of Rhodamine B, while C_e (mg L^{-1}) indicates the concentration of Rhodamine B at equilibrium. Fig. S2† shows the absorbance readings recorded at different concentrations of Rhodamine B solutions (0 μM, 10 μM, 20 μM, 30 μM, 50 μM), which were then used to construct a calibration curve based on the Beer–Lambert law. The UV-Vis spectrum of Rhodamine B presents a prominent peak at 533 nm, corresponding to the wavelength of maximum absorption.

2.5 Adsorption kinetics

The kinetics of adsorption are determined by analysing experimental data collected during an adsorption process. Several kinetic models, including pseudo-first order and pseudo-second order models, can be used to describe the behaviour of adsorption over time. The first-order model describes adsorption as a reaction of the first order, where the rate of adsorption is directly proportional to the concentration of the remaining solute. The equation for the pseudo first-order model is typically expressed as:

$$\ln(q_e - q_t) = \ln(q_e) - k_1 t \quad (4)$$

where q_e is the equilibrium adsorption capacity, q_t is the adsorption capacity at time t, k_1 is the first-order rate constant, and t represents time. On the other hand, the second-order model takes into account not only the solute concentration but also the available surface area for adsorption. The equation for the second-order model is typically represented as:

$$\frac{t}{q_t} = \left(\frac{1}{q_e}\right) \times t + \frac{1}{(k_2 q_e^2)} \quad (5)$$

where t represents time, q_t is the concentration of the solute at time t, q_e denotes the equilibrium adsorption capacity, and k_2 is the second-order rate constant.

3 Results and discussion

3.1 HTC data

Assuming that the overall reaction follows first-order kinetics and the Arrhenius temperature relation, the empirical parameters were obtained by fitting the model to the experimental data. In this and most other studies, the fitted parameter is assigned a value of 14.75, which corresponds to a reaction rate

Table 1 Hydrochar yields at different $\log R_0$

Sample	$\log R_0$	HC yields (wt%)
SM1 (HC_{180-60})	4.13	22.82
SM2 (HC_{240-60})	5.90	21.02
SM3 (HC_{300-60})	7.66	12.98
SM4 ($HC_{180-180}$)	4.61	24.18
SM5 ($HC_{240-180}$)	6.37	18.14
SM6 ($HC_{300-180}$)	8.14	13.22
SM7 ($HC_{180-300}$)	4.83	20.54
SM8 ($HC_{240-300}$)	6.59	16.19
SM9 ($HC_{300-300}$)	8.36	11.33

that doubles for every 10 °C increase in temperature. The severity factor values were then correlated with the percent yields, as reported in Table 1 and Fig. 1.

Fig. 1 illustrates that lower $\log R_0$ values result in higher hydrochar yield percentages. Recent studies have indicated that residence time is a critical factor in hydrochar formation, as longer residence times increase reaction severity. While temperature has a more significant effect on solid product recovery, residence time also plays a role, albeit to a lesser degree. A shorter residence time led to a higher solid hydrochar content (60 and 180 minutes), which decreased gradually with increasing residence time (300 minutes). Additionally, the simultaneous effect of reaction time and temperature significantly influences yield. Decreasing the reaction temperature resulted in higher yields, with the maximum yield of 24.18% achieved at 180 °C and 3 hours of reaction time. The anomalous trend of the increase in hydrochar yield after 180 min, compared to 1 hour and 5 hours, could be attributed to several factors: the HTC process involves several chemical transformations, such as hydrolysis, dehydration, and condensation reactions. These reactions require sufficient time to occur and reach equilibrium.[37] Therefore, the initial stages of the reaction can involve the breakdown of the labile components, while longer reaction times allowed for the conversion of more recalcitrant components into carbonaceous materials until a plateau.[38] A decreasing trend in yield was observed at 240 °C, inversely proportional to reaction duration, which is directly proportional to $\log R_0$. At 300 °C, the yield was almost similar for reaction times of 60 and 180 minutes but lower for 300 minutes. Compared to other biomasses, the response of algae to increasing reaction temperatures shows a distinct pattern. Recent research suggests that the solid content of seaweed hydrochar decreases under more severe temperature conditions.[37,39,40] This outcome is potentially attributed to increased solubilization of the biomass, leading to the release of compounds into the liquid phase. Furthermore, the higher activation energy required to break the chemical bonds of the biomass components into their corresponding monomers may facilitate further decomposition of the solid residue.[38]

3.2 Characterization data

Fig. 2a, S3a, and b† illustrate the obtained Infrared spectra. As observed, all hydrochar samples exhibited similar absorption bands. The variations in the intensity of the absorption peaks are not reflected in the FTIR spectra. The wide band located between 3000 cm⁻¹ and 3700 cm⁻¹ is attributed to the stretching vibration of the hydroxyl groups. The intensity of this band decreases at 240 °C and 300 °C, probably caused by dehydration reactions occurring at higher temperatures. The small peak at 3330 cm⁻¹ particularly evident at 180 °C could be attributed to the symmetrical and asymmetrical vibrations of
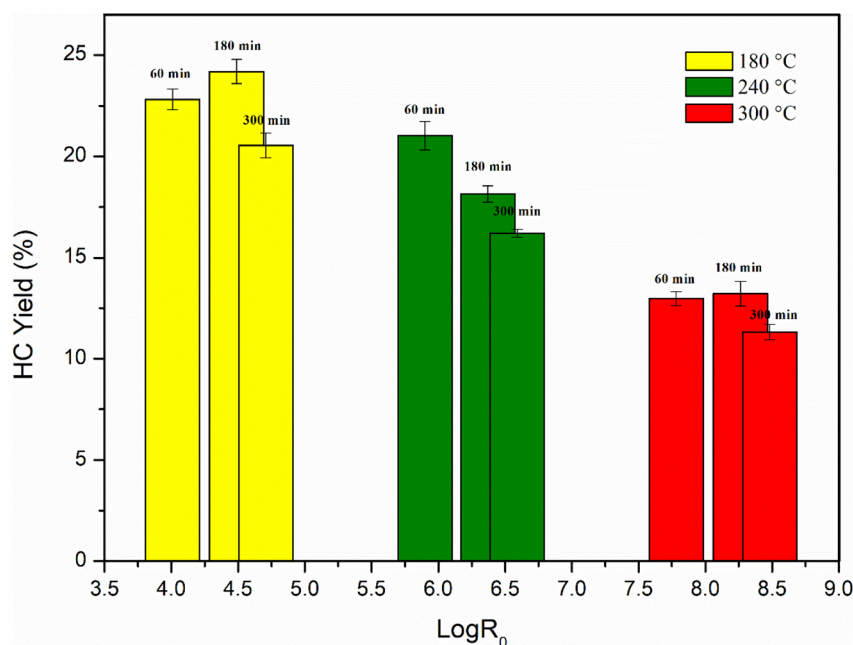

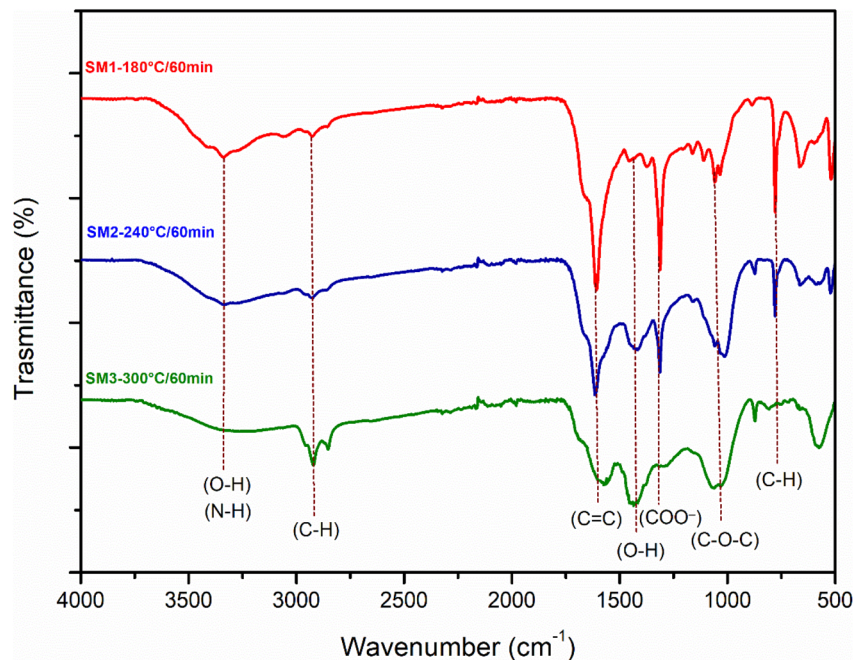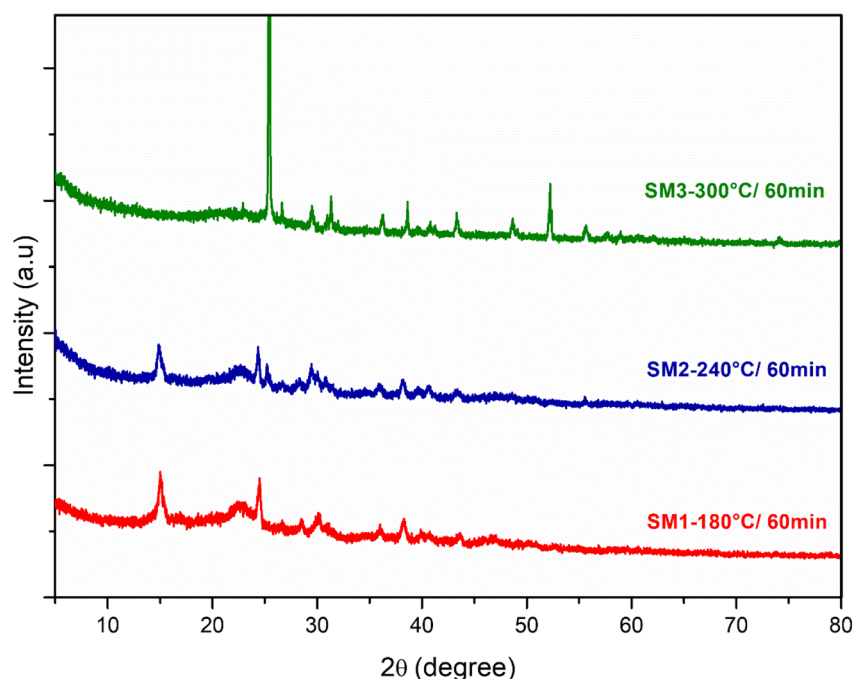**Fig. 1** Percentage yield of hydrochar as a function of $\log R_0$, sd. ≤1.

Fig. 2 FT-IR spectra of hydrochar obtained from the hydrothermal process of algae at three different reaction temperatures (180 °C, 240 °C, 300 °C) and a reaction time of 60 min.

the N–H group or O–H group. The bands located at 2925 cm^{-1} and 2850 cm^{-1} are ascribed to the stretching vibrations of the aliphatic C–H groups and strain vibrations. The transmittance intensity of these bands increases with increasing temperature, probably due to the reduction of aromatic O and C following the carbonization process.[41] The peak at 1613 cm^{-1} could be responsible for the stretching of C=C and C=O, which agrees with the XPS results. The peak at 1490 cm^{-1} suggests the presence of amino groups. The signal at 1300 cm^{-1} could be related to the stretching vibration of the aromatic ring, which is in agreement with the XRD spectra showing the loss of the amorphous structure. The band around 1061 cm^{-1} can be

Fig. 3 XRD spectra of hydrochar obtained from the hydrothermal process of algae at three different reaction temperatures (180 °C, 240 °C, 300 °C) and a reaction time of 60 min.
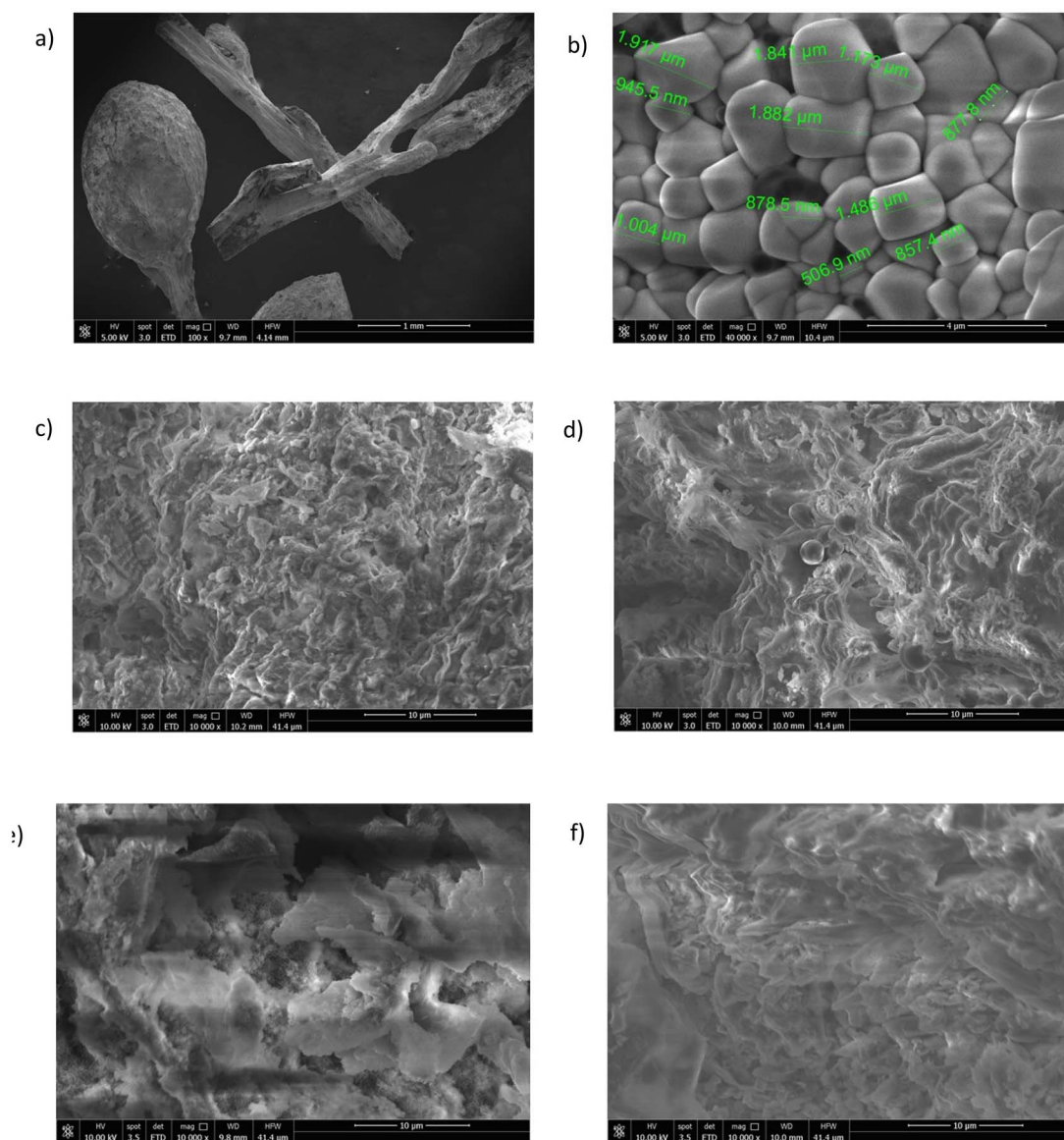
Fig. 4 SEM images of *Sargassum muticum*: (a) fragments of the thallus before the process; (b) magnification of the thallus surface showing algal cells; (c) sample SM4; (d) sample SM5; (e) sample SM7; (f) sample SM8.

ascribed to the β-glycosidic bond of cellulose and hemicellulose.[42] This band is reduced as the reaction time increases (also in accordance with the XRD outcomes). As observed for other hydrochars derived from biomass,[14,43] FTIR spectra indicate that the reaction time has no influence on the structural properties of the samples, whereas temperature plays a crucial role in determining the surface functional groups due to the rearrangement of chemical bonds, the reaction of dehydration, the degree of carbonization, and the decomposition. Furthermore, the lack of significant changes in surface functional groups over time suggests that the composition of hydrochars remains relatively stable within the duration of the experiment.

Fig. 3 and S4a and b† show the X-ray diffraction spectra (XRD) of the hydrochars produced under different HTC conditions of time (60, 180 and 300 min) and temperature (180, 240,

300 °C). The samples showed similar XRD patterns: as reported in the literature, the diffraction peaks at 2θ 15 and 25 represent the ordered structure of microcrystalline cellulose.[44] With the increase in the reaction temperature, the peak at 15 2θ disappears, underlining that the cellulose components begin to degrade and its microcrystalline structure gives way to a more amorphous one. The reaction time doesn't play a fundamental role, however the hydrochar obtained at 240 °C and 300 °C for 300 minutes showed a stronger peak at the 25.79 2θ angle, demonstrating the formation of carbon layer planes which may be indicative of the disordered diffraction plane of the graphite.[45] The XRD analysis is in agreement with that observed previously for other biomasses, in fact, the spectra show the presence of lower intensity peaks indicative of inorganic compounds derived from algal ash content:[46] in particular the

Table 2 Surface area, pore radius and pore volume of hydrochar samples

Sample	Surface area ($m^2\ g^{-1}$)	Pore radius (Å)	Pore volume (cc g^{-1})
SM1	29.09	20.856	0.078
SM2	60.86	21.774	0.126
SM3	38.40	21.002	0.135
SM4	21.77	25.125	0.027
SM5	29.84	17.220	0.063
SM6	13.18	16.622	0.031
SM7	18.81	16.992	0.012
SM8	22.02	18.072	0.057
SM9	26.40	20.151	0.081

2θ diffraction peaks at 41.13 and 44 are assignable to phosphates of Al and Cu, while the peak at 25.32 indicates the presence of $CaSO_4$.[38]

The SEM images of the hydrochar samples collected at varying magnifications are illustrated in Fig. 4. These images are indicative of the porous structure of the hydrochar sample. To gain insights into the morphology of the algae, SEM images of the raw material were also obtained (Fig. 4a and b). In Fig. 4b, several spherical aggregations with an average diameter of 874 μm and a smooth surface without whiskers are evident. As shown in Fig. 4c–f at the same magnification, variations in the reaction conditions lead to the formation of cracks on the surface and the spheres become smaller microspheres. Longer residence time (300 min, Fig. 4e and f) had a visible effect on surface morphology because cellulose and hemicellulose did not completely react at shorter residence times. A longer residence time resulted in the polymerization of monomers present in the liquid phase, leading to the formation of secondary hydrochar with a polyaromatic structure.[47] As reported in the literature for lignocellulosic biomasses, the residence time heavily influences the secondary hydrochar formation because the fading of fragments requires extensive polymerization.[48] The abundant presence of C and O, as well as elements such as Mg, K, and Ca, which are widely dispersed in the matrix, was confirmed by EDX spectroscopy (Fig. S5†). These elements were particularly abundant in the samples obtained after 60 min of treatment.

The porous structure of hydrochar is formed through carbonization, which involves the release of volatile matter: as the matter is liberated, pores and cracks emerge on the surface of the hydrochar. As shown in Table 2 and according to the literature,[45,49] BET surface areas were relatively low. As reported by Qin et al.,[50] the low surface area of hydrochar can be attributed to dehydration, polymerization and condensation reactions during the hydrothermal treatment, which hinder pore formation. In contrast to the hydrochars described in the literature, these samples, especially those obtained after 60 minutes of treatment have a good surface area with the largest surface area exhibited by the sample SM2. Moreover, the samples obtained at 240 °C show the highest values compared to the other samples.

The surface compositions of the hydrochar, especially the three hydrochars formed after 60 min at various temperatures (SM1, SM2 and SM3) were studied by XPS. The results are compiled in Fig. 5. It clearly and logically appears that the materials are mainly composed of carbon, oxygen and nitrogen. However, small traces of calcium and silicium were detected. While the presence of calcium is consistent with the previously
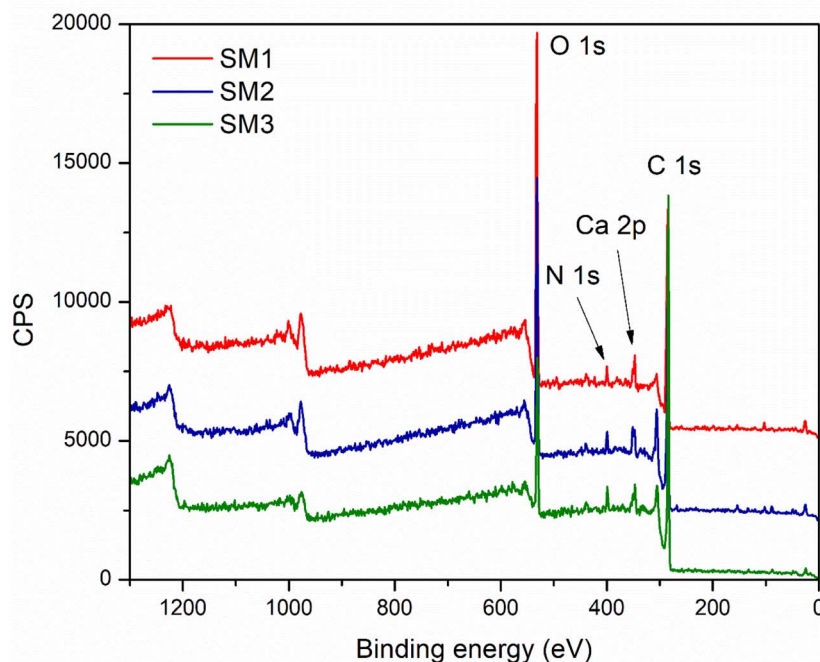

Fig. 5 Full-scale XPS survey scan of the hydrochars SM1, SM2, and SM3.

Table 3 XPS elements and relative percentages

SM1			SM2			SM3		
O	1s	29.85%	O	1s	24.66%	O	1s	13.86%
C	1s	64.66%	C	1s	69.07%	C	1s	82.23%
N	1s	1.84%	N	1s	2.63%	N	1s	2.47%
Ca	2p	1.98%	Ca	2p	2.55%	Ca	2p	1.44%
Si	2p	1.67%	Si	2p	1.08%			

discussed results, the detection of silicium was ascribed to a contamination of the hydrochars. The analysis of the C 1s spectra reveals the existence of several functional groups such as aromatic and aliphatic C–C/C–H, carboxyl and carbonyl groups. The nitrogen spectra seem to indicate the presence of quaternary nitrogen species. This could derive from the biomolecules in the starting materials, which possess this kind of nitrogen. As expected, the XPS characterization led to valuable information about the surface chemistry of the hydrochars, which is needed to evaluate their potential in various applications including in environmental or energy-related fields.[51] The percentages of the elements are summarized in the following Table 3. It can be noted that increasing the synthesis temperature leads to an enrichment of carbon combined with an important loss of oxygen.

3.3 Adsorption of Rhodamine B dye

According to the literature,[45,52] hydrochar does not show high adsorbing power probably due to the low surface area, and therefore it could be activated by chemical and physical processes. In this study, the hydrochars obtained after 60 minutes at different temperatures exhibited superior surface areas, so they were used without any activation, showing an excellent adsorption

capacity. The adsorption mechanism could be due to the surface area of the samples under investigation. The results are in agreement, showing that the SM2 sample, with the highest surface area, exhibited the best response, even at low concentrations. Nevertheless, all the samples investigated displayed good adsorption performance. Therefore, in addition to the adsorption mechanism, a surface chemical interaction between the polar groups of the hydrochar and Rhodamine B could also contribute, indicating the existence of hydrogen bonding[45] and π–π interactions between the aromatic rings.[53]

3.3.1 Effect of hydrochars amount. In this study, the effect of adsorbent dosage was investigated by using different amounts of hydrochar (5 mg, 10 mg, 30 mg, 50 mg, and 100 mg) at 25 °C in 50 mL of Rhodamine B solution (50 µM), under stirring for 60 minutes. (Fig. 6) illustrates that as the adsorbent dosage increases from 5 to 30 mg, the dye removal rate increases for all the samples, reaching 67.02% for SM1, 83.6% for SM2, and 71.12% for SM3. However, as the dosage of hydrochars is further increased from 30 to 100 mg, the percentage of removal decreases, indicating probably the saturation of adsorption sites. This observation suggests that the availability of active sites for the adsorption of Rhodamine B is directly proportional to the quantity of adsorbents employed in the experiment. Accordingly, an increase in the dosage of adsorbents leads to a linear increase in the number of available sites and thus to an increase in the amount of Rhodamine B adsorbed by the hydrochars. However, beyond a dosage of 30 mg, no significant change is observed, indicating that adsorption sites have reached equilibrium. Therefore, 30 mg was chosen as the optimal dosage for subsequent studies.

3.3.2 Effect of contact time. Fig. 7 presents the effect of contact time (from 5 to 60 min) on Rhodamine B adsorption. The experiments were conducted at 25 °C with an adsorbent
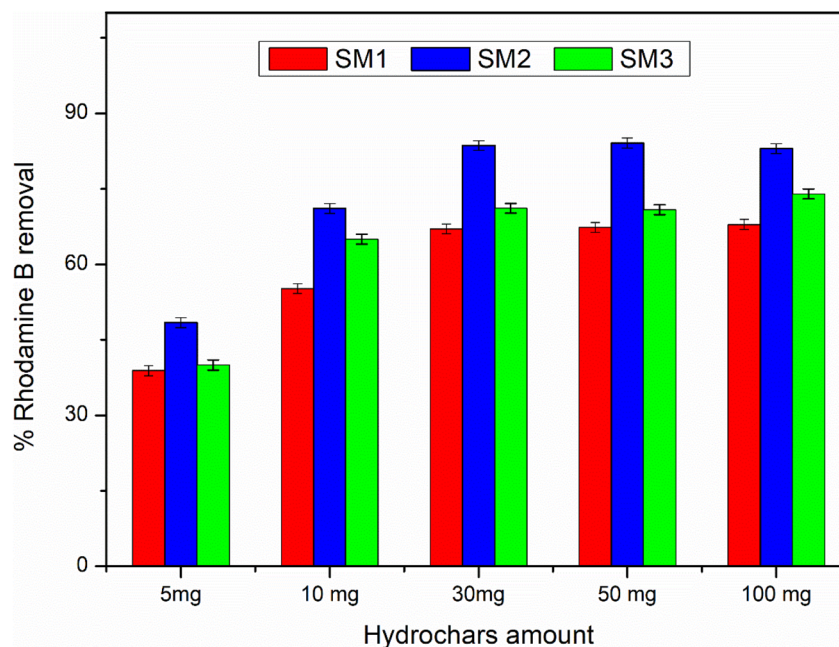

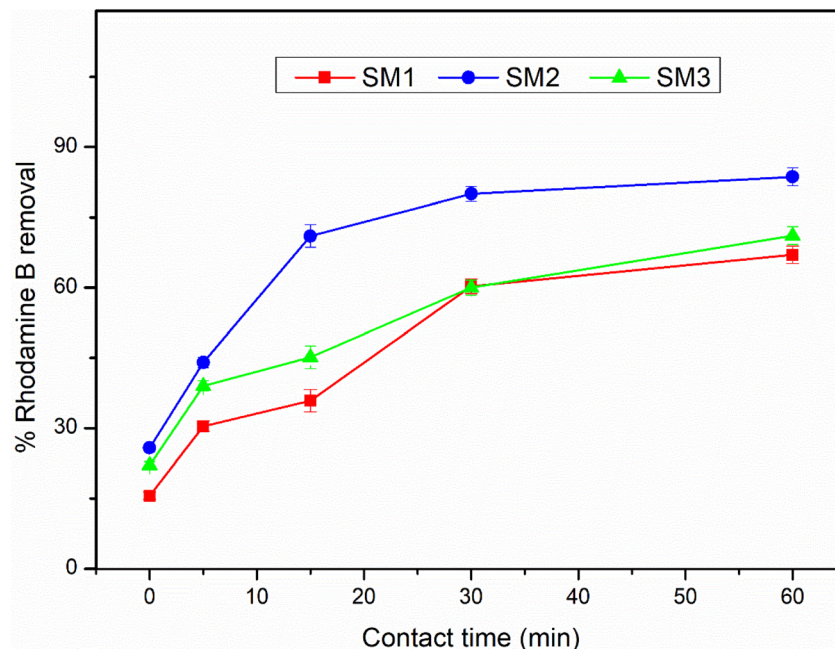**Fig. 6** Adsorbent amount effect on % Rhodamine B removal, sd. ≤1.
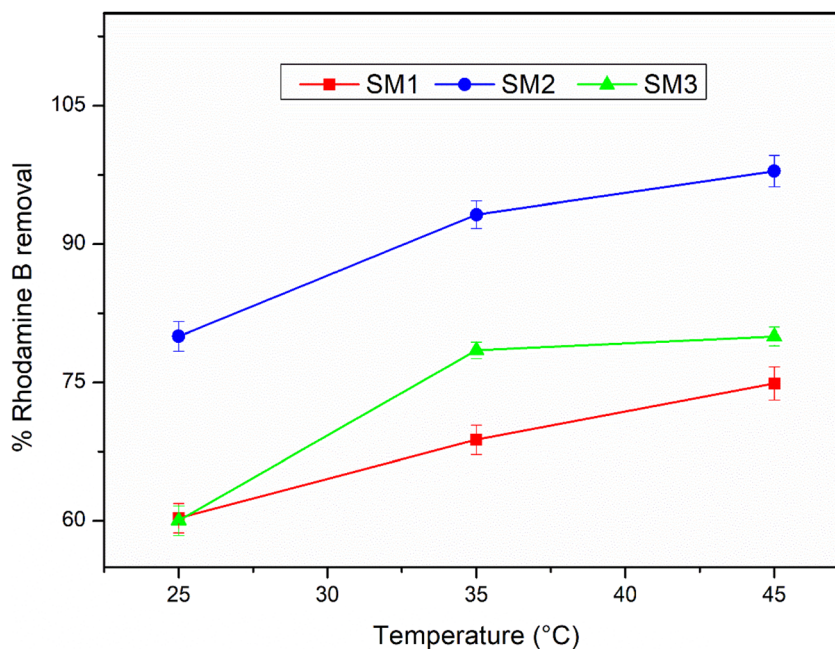
Fig. 7 Time effect on % Rhodamine B removal, sd. ≤2.

Fig. 8 Temperature effect on % Rhodamine B removal, sd. ≤3.

amount of 30 mg for all samples, and 50 mL of Rhodamine B solution with a concentration of 50 μM, under stirring. The adsorption of Rhodamine B rapidly increased in the first 30 minutes, followed by a gradual increase up to 60 minutes, with the highest removal rate achieved by SM2, increasing from 25.8% to almost 84%. The adsorption capacity of the hydrochar was efficient, as indicated by the percentage removal of the adsorbent at time zero, and the high affinity for the contaminant. Fig. S6† displays the solutions and the significant color

quenching resulting from the adsorption of the organic compound by hydrochar SM2.

3.3.3 Effect of temperature. The effect of the operating temperature on the removal of Rhodamine B [50 μM] was evaluated at three temperature values (25 °C, 35 °C, and 45 °C), establishing the reaction time as 30 minutes. As depicted in Fig. 8, at the maximum temperature the samples showed 74.9%, 97.8%, and 80% Rhodamine B removal respectively for SM1, SM2 and SM3. Therefore, the removal efficiency is higher when the

Table 4 Adsorption kinetics' parameters

Samples	Pseudo-first order kinetic model			Pseudo-second order kinetic model		
	q_e (mg g^{-1})	k_t (min^{-1})	R^2	q_e (mg g^{-1})	k_t (g mg^{-1} min^{-1})	R^2
SM1	13.59	0.065	0.92	17.29	0.009	0.95
SM2	13.98	0.094	0.94	20.77	0.019	0.99
SM3	11.11	0.046	0.97	17.69	0.012	0.98

Table 5 Comparison between *Sargassum*-derived adsorbents

Samples	Pollutants	Technique	% removal	Ref.
Sargassum muticum hydrochar activated by KOH treatment	Methylene blue	Adsorption	91	25
Dried *Sargassum muticum*	Cr(VI)	Adsorption	84.4	55
Dried *Sargassum muticum* treated with CaCl$_2$	Methylene blue	Adsorption	97	56
Dried *Sargassum muticum* treated with HCl			98	
Dried *Sargassum muticum* treated with H$_2$CO			98	
Dried *Sargassum muticum*	Hg(II)	Adsorption	86	57
Dried and grinded *Sargassum muticum*	Methylene blue	Adsorption	96.13	58
	Pb(II)		96	
Dried and sieved *Sargassum ilicifolium*	Hydrazine	Adsorption	94	59
Sargassum muticum fabricated AgNPs	Methylene blue	Adsorption	63.5	60
	Methyl orange		66.5	
Sargassum oligocystum treated with CaCl$_2$	Cr(VI)	Adsorption	>95	61
Sargassum horneri hydrochar	Methylene blue	Adsorption	99	62
Dried and sieved *Sargassum hemiphyllum*	Methylene blue	Adsorption	>86	63
Dried and grinded *Sargassum dentifolium*	Methylene blue	Adsorption	99.2	64
Dried *Sargassum glaucescens*	Acid black 1	Adsorption	94	65
Sargassum fusiforme hydrochar	Heavy metals	Adsorption	>86	66
Dried *Sargassum hemiphyllum*	Ni(II)	Adsorption	67.4	67
Sargassum honeri magnetically modified	Dyes pollutants	Adsorption	>90	68
Sargassum muticum hydrochar SM1	Rhodamine B	Adsorption	75	This work
Sargassum muticum hydrochar SM2			98	
Sargassum muticum hydrochar SM3			80	

temperature is high, indicating that the temperature affects the enhancement of the chemical–physical bonds between the adsorbate and the adsorbent.

3.4 Adsorption kinetic results

The adsorption kinetic values of q_e, k_t and R^2 were evaluated and calculated from eqn (3) and eqn (4) and the data are plotted in Fig. S7.† The corresponding results are summarized in Table 4. The calculated pseudo-second order correlation coefficient (R^2) values were superior to those obtained from the pseudo-first order kinetic model for all the samples. This suggests that the pseudo-second order model fits well with the experimental data, supporting that the hydrochar-mediated adsorption process is primarily governed by chemisorption,[54] involving the formation of chemical bonds between the polar groups and aromatic groups present on the hydrochar surface and Rhodamine B molecules in solution.

3.5 Comparison with literature data

The table below (Table 5) displays the adsorbent potential of various samples derived from *Sargassum muticum* and other *Sargassum*-based adsorbents. Its purpose is to compare the adsorptive capacities of the hydrochars obtained in this study with

those reported in recent research. According to the available data, there is limited literature on the use of hydrochars derived from *Sargassum muticum* for direct adsorption purposes. However, the obtained results are comparable to those obtained from other macroalgae sources or even chemically treated *Sargassum muticum*. These promising findings show that these hydrochars have the potential to be exploited as effective adsorbents without the requirement of additional physical or chemical activation processes, thus promoting the use of environmentally friendly materials.

4 Conclusions

In this study, thalli of the alga *Sargassum muticum* were converted to hydrochar by hydrothermal carbonization, and the role of temperature and residence time was investigated, showing a maximum hydrochar yield at 180 °C after 180 min. Based on the characterization data, the samples contained a large number of oxygen, carboxyl, and amino functional groups and showed a stable mesoporous structure. The SM2 sample showed the highest surface area and it proved to be the best adsorbent for Rhodamine B in water with a removal rate of up to 98% when left at 45 °C for 30 minutes.

The present research fits in a larger project dealing with the exploitation of algal biomass, such as those produced by blooms of natural populations of invasive algae in dystrophic environments. In this scenario, huge algal biomasses, which disturb the equilibrium of the ecosystem, the wellness of native species, the provision of ecosystem services, and the realization of human activities, are usually treated as waste. A potential use of unwanted algal biomasses is suggested, which involves their conversion into a valuable resource, thereby laying the foundations for a sustainable, economic, and efficient process.

Conflicts of interest

There are no conflicts to declare.

References

1 J. Wehr, *J. Phycol.*, 2011, **47**, 436–438.

2 G. Genovese, C. Faggio, C. Gugliandolo, A. Torre, A. Spanò, M. Morabito and T. L. Maugeri, *Mar. Environ. Res.*, 2012, **73**, 1–6.

3 F. Marino, G. Di Caro, C. Gugliandolo, A. Spanò, C. Faggio, G. Genovese, M. Morabito, A. Russo, D. Barreca, F. Fazio and A. Santulli, *Front. Physiol.*, 2016, **7**, 459–470.

4 C. Rizzo, G. Genovese, M. Morabito, C. Faggio, M. Pagano, A. Spanò, V. Zammuto, S. Minicante, A. Manghisi, R. Cigala, F. Crea, F. Marino and C. Gugliandolo, *J. Pure Appl. Microbiol.*, 2017, **11**, 1695–1706.

5 M. Bilal and H. M. N. Iqbal, *Mar. Drugs*, 2018, **16**(2), 65–81.

6 V. Zammuto, M. G. Rizzo, A. Spanò, D. Spagnuolo, A. Di Martino, M. Morabito, A. Manghisi, G. Genovese, S. Guglielmino, G. Calabrese, F. Capparucci, C. Gervasi, M. S. Nicolò and C. Gugliandolo, *Algal Res.*, 2022, **63**, 102646.

7 C. Solidoro, V. Bandelj, F. A. Bernardi, E. Camatti, S. Ciavatta, G. Cossarini, C. Facca, P. Franzoi, S. Libralato and D. M. Canu, *Coastal Lagoons: Critical Habitats of Environmental Change*, 2010, pp. 483–511.

8 C. Louime, J. Fortune and G. Gervais, *Am. J. Environ. Sci.*, 2017, **13**, 58–64.

9 V. Bressi, A. M. Balu, D. Iannazzo and C. Espro, *Curr. Opin. Green Sustainable Chem.*, 2023, **40**, 100742.

10 L. Gnanasekaran, A. K. Priya, S. Thanigaivel, T. K. A. Hoang and M. Soto-Moscoso, *Fuel*, 2023, **331**, 125668.

11 C. Yao, P. Wu, Y. Pan, H. Lu, L. Chi, Y. Meng, X. Cao, S. Xue and X. Yang, *Bioresour. Technol.*, 2016, **216**, 381–390.

12 A. Funke and F. Ziegler, *Biofuels, Bioprod. Biorefin.*, 2010, **4**, 160–177.

13 V. Bressi, A. Ferlazzo, D. Iannazzo and C. Espro, *Nanomaterials*, 2021, **11**, 1120.

14 A. Satira, E. Paone, V. Bressi, D. Iannazzo, F. Marra, P. S. Calabrò, F. Mauriello and C. Espro, *Appl. Sci.*, 2021, **11**, 10983.

15 T. Len, V. Bressi, A. M. Balu, T. Kulik, O. Korchuganova, B. Palianytsia, C. Espro and R. Luque, *Green Chem.*, 2022, **24**, 7801–7817.

16 Y. H. Chan, S. S. M. Lock, B. L. F. Chin, M. K. Wong, A. C. M. Loy, S. Y. Foong, C. L. Yiin and S. S. Lam, *Bioresour. Technol.*, 2023, 129061.

17 M. T. Reza, J. Andert, B. Herklotz, D. Busch, J. Pielert, J. Lynam and J. Mumme, *Appl. Bioenergy*, 2014, **1**, 11–29.

18 J. Yu, T. Tang, F. Cheng, D. Huang, J. L. Martin, C. E. Brewer, R. L. Grimm, M. Zhou and H. Luo, *MethodsX*, 2021, **8**, 101263.

19 M.-M. Titirici and M. Antonietti, *Chem. Soc. Rev.*, 2010, **39**, 103–116.

20 V. Bressi, I. Chiarotto, A. Ferlazzo, C. Celesti, C. Michenzi, T. Len, D. Iannazzo, G. Neri and C. Espro, *ChemElectroChem*, 2023, e202300004.

21 Q. Ye, Z. Huang, P. Wu, J. Wu, J. Ma, C. Liu, S. Yang, S. Rehman, Z. Ahmed, N. Zhu and Z. Dang, *J. Hazard. Mater.*, 2020, **388**, 122120.

22 M. A. Mohammed, A. Shitu and A. Ibrahim, *Res. J. Chem. Sci.*, 2014, **4**, 91–102.

23 M. H. Park, S. Jeong and J. Y. Kim, *J. Environ. Chem. Eng.*, 2019, **7**, 103039.

24 L. García, J. C. Leyva-Díaz, E. Díaz and S. Ordóñez, *Sci. Total Environ.*, 2021, **780**, 146554.

25 C. Chambers, S. Saha, S. Grimes, J. Calhoun and M. T. Reza, *Biomass Convers. Biorefin.*, 2023, DOI: **10.1007/s13399-023-04326-2**.

26 L. Ding, B. Zou, W. Gao, Q. Liu, Z. Wang, Y. Guo, X. Wang and Y. Liu, *Colloids Surf., A*, 2014, **446**, 1–7.

27 Y.-Y. Cheng and T.-H. Tsai, *J. Agric. Food Chem.*, 2017, **65**, 1078–1085.

28 F. Anjum, A. M. Asiri, M. A. Khan, M. I. Khan, S. B. Khan, K. Akhtar, E. M. Bakhsh, K. A. Alamry, S. Y. Alfifi and S. Chakraborty, *J. Mater. Res. Technol.*, 2021, **15**, 3171–3191.

29 M. E. Mahmoud, M. S. Abdelwahab and G. A. A. Ibrahim, *Mater. Chem. Phys.*, 2023, **301**, 127638.

30 A. Bilgic, *J. Alloys Compd.*, 2022, **899**, 163360.

31 J. Huang, Y. Feng, H. Xie, P. Wu, M. Wang, B. Wang, Q. Zhang, S. Zhang and Z. Liu, *Biochar*, 2023, **5**, 12.

32 Z. Liu, Z. Wang, H. Chen, T. Cai and Z. Liu, *Environ. Pollut.*, 2021, **268**, 115910.

33 Y. Hou, G. Huang, J. Li, Q. Yang, S. Huang and J. Cai, *J. Anal. Appl. Pyrolysis*, 2019, **143**, 104694.

34 Z. Lin, R. Wang, S. Tan, K. Zhang, Q. Yin, Z. Zhao and P. Gao, *J. Environ. Manage.*, 2023, **334**, 117503.

35 R. P. Overend, E. Chornet, J. A. Gascoigne, B. S. Hartley, P. M. A. Broda and P. J. Senior, *Philos. Trans. Royal Soc. A*, 1997, **321**, 523–536.

36 H. A. Ruiz, M. Galbe, G. Garrote, D. M. Ramirez-Gutierrez, E. Ximenes, S.-N. Sun, D. Lachos-Perez, R. M. Rodríguez-Jasso, R.-C. Sun, B. Yang and M. R. Ladisch, *Bioresour. Technol.*, 2021, **342**, 125961.

37 J. de S. Castro, P. P. Assemany, A. C. de O. Carneiro, J. Ferreira, M. M. de Jesus Júnior, F. de Á. Rodrigues and M. L. Calijuri, *Sci. Total Environ.*, 2021, **768**, 144480.

38 H. Liu, Y. Chen, H. Yang, F. G. Gentili, U. Söderlind, X. Wang, W. Zhang and H. Chen, *Fuel*, 2019, **249**, 441–448.

39 C. G. Khoo, M. K. Lam, A. R. Mohamed and K. T. Lee, *Environ. Res.*, 2020, **188**, 109828.

40 P. G. Del Río, B. Gullón, A. Pérez-Pérez, A. Romaní and G. Garrote, *Bioresour. Technol.*, 2021, **340**, 125733.

41 B. Biswas, Y. Bisht, J. Kumar, S. R. Yenumala and T. Bhaskar, *Biomass Convers. Biorefin.*, 2022, **12**, 91–101.

42 R. D. Kale and V. G. Gorade, *Int. J. Biol. Macromol.*, 2019, **124**, 25–33.

43 M. Röhrdanz, T. Rebling, J. Ohlert, J. Jasper, T. Greve, R. Buchwald, P. von Frieling and M. Wark, *J. Environ. Manage.*, 2016, **173**, 72–78.

44 H. Rustamaji, T. Prakoso, J. Rizkiana, H. Devianto, P. Widiatmoko and G. Guan, *Int. J. Renewable Energy Dev.*, 2022, **11**, 403–412.

45 S. Masoumi and A. K. Dalai, *J. Cleaner Prod.*, 2020, **263**, 121427.

46 J. Clemente, S. Beauchemin, Y. Thibault, T. MacKinnon and D. Smith, *ACS Omega*, 2018, **3**, 6931–6944.

47 C. He, A. Giannis and J.-Y. Wang, *Appl. Energy*, 2013, **111**, 257–266.

48 T. Wang, Y. Zhai, Y. Zhu, C. Li and G. Zeng, *Renewable Sustainable Energy Rev.*, 2018, **90**, 223–247.

49 C. Espro, A. Satira, F. Mauriello, Z. Anajafi, K. Moulaee, D. Iannazzo and G. Neri, *Sens. Actuators, B*, 2021, **341**, 130016.

50 T. Qin, M. Song, K. Jiang, J. Zhou, W. Zhuang, Y. Chen, D. Liu, X. Chen, H. Ying and J. Wu, *RSC Adv.*, 2017, **7**, 37112–37121.

51 S. Guo, Y. Wang, X. Wei, Y. Gao, B. Xiao and Y. Yang, *Environ. Sci. Pollut. Res.*, 2020, **27**, 18866–18874.

52 H. M. El-Bery, M. Saleh, R. A. El-Gendy, M. R. Saleh and S. M. Thabet, *Sci. Rep.*, 2022, **12**, 5499.

53 Z. Hou, Y. Tao, T. Bai, Y. Liang, S. Huang and J. Cai, *J. Environ. Chem. Eng.*, 2021, **9**, 105757.

54 L. Xie, K. Ding, Y. Liu, M. Zou and C. Han, *Open J. Yangtze Oil Gas*, 2019, **04**, 286–301.

55 Y. González Bermúdez, I. L. Rodríguez Rico, E. Guibal, M. Calero de Hoces and M. Á. Martín-Lara, *Chem. Eng. J.*, 2012, **183**, 68–76.

56 E. Rubin, P. Rodriguez, R. Herrero, J. Cremades, I. Barbara and M. E. Sastre de Vicente, *J. Chem. Technol. Biotechnol.*, 2005, **80**, 291–298.

57 L. Carro, J. L. Barriada, R. Herrero and M. E. Sastre de Vicente, *Chem. Eng. J.*, 2013, **229**, 378–387.

58 Y. Hannachi and A. Hafidh, *Int. J. Environ. Sci. Technol.*, 2020, **17**, 3875–3890.

59 R. Tabaraki and A. Nateghi, *Environ. Prog. Sustainable Energy*, 2016, **35**, 1450–1457.

60 S. Trivedi, M. A. Alshehri, A. T. Aziz, C. Panneerselvam, H. A. Al-Aoh, F. Maggi, S. Sut and S. Dall'Acqua, *S. Afr. J. Bot.*, 2021, **139**, 432–441.

61 R. Foroutan, R. Mohammadi and B. Ramavandi, *Korean J. Chem. Eng.*, 2018, **35**, 234–245.

62 S. Soroush, F. Ronsse, A. Verberckmoes, F. Verpoort, J. Park, D. Wu and P. M. Heynderickx, *Biomass Convers. Biorefin.*, 2019, DOI: 10.1007/s13399-022-02365-9.

63 J. Liang, J. Xia and J. Long, *Water Sci. Technol.*, 2017, **76**, 1574–1583.

64 R. M. Moghazy, A. Labena and Sh. Husien, *Int. J. Biol. Macromol.*, 2019, **134**, 330–343.

65 E. Daneshvar, M. Kousha, M. Jokar, N. Koutahzadeh and E. Guibal, *Chem. Eng. J.*, 2012, **204–206**, 225–234.

66 K.-M. Poo, E.-B. Son, J.-S. Chang, X. Ren, Y.-J. Choi and K.-J. Chae, *J. Environ. Manage.*, 2018, **206**, 364–372.

67 X. Fan, J. Xia and J. Long, *Environ. Prog. Sustainable Energy*, 2019, **38**, S250–S259.

68 R. Angelova, E. Baldikova, K. Pospiskova, Z. Maderova, M. Safarikova and I. Safarik, *J. Cleaner Prod.*, 2016, **137**, 189–194.